A novel resilient state of charge balancing method for distributed storage systems based autonomous microgrids

Sidlawendé Ouoba, Azeddine Houari, Mohamed Machmoum, Josep M Guerrero

A Novel Resilient State of Charge Balancing Method for Distributed Storage Systems based Autonomous Microgrids

Sidlawendé V. M. Ouoba [1]*, Azeddine Houari [1], Mohamed Machmoum [1], Josep M. Guerrero[2]

[1] Nantes Université, Institut de Recherche en Énergie Électrique de Nantes Atlantique, IREENA, UR 4642, F-44600 Saint-Nazaire, France

[2] Aalborg University, Villum Center for Research on Microgrids, CROM, Aalborg, Denmark

*sidlawende.ouoba@etu.univ-nantes.fr

Abstract—In order to reduce the number of charge/discharge cycles of distributed energy storage systems (DESSs) to extend their lifespan, a State-of-Charge (SoC) balancing control is used. In conventional SoC balancing strategies, a local integral control is generally introduced in each DESS to ensure SoC equalization and Distributed Generators (DGs) frequency restoration. These strategies increase the system order and have a constraining bandwidth that may lead to stability issues. The few methods in which a local integrator is not added generally result in poor performance of the SoC synchronization strategy and frequency restoration, with the inability to eliminate static error. In this proposal, a novel resilient distributed control is proposed to ensure an effective SoC balancing of DESSs and frequency restoration with high performance without increasing the system order with a local integral control. The dynamic average consensus is modified to evaluate the participation level of each DESS in order to determine the active power references to synchronize the SoCs of the DESSs. These active power references are chosen to regulate the DG frequency to the nominal frequency of the MG. Therefore, the proposed method ensures SoC balancing with automatic frequency regulation and accurate output power sharing performance. Only voltage restoration control is added for

DGs voltage regulation. In this distributed control architecture, SoC equalization as well as voltage/frequency restoration are performed only with local DG information and information from their neighbors. Simulations and then experimental results are performed to verify the effectiveness of the proposed method in discharging mode, in charging mode, in the presence of intermittent renewable energy sources, in the case of communication failure, in the case of communication delay, in the case of load variation, and in the case of "plug and play". Comparisons were also made with two SoC balancing strategies from the literature.

Keywords—Distributed Energy Storage System, Distributed control, Consensus Control, Power management, SoC balancing.

1. Introduction

Microgrids (MG) have emerged as the most promising solution to meet the environmental and energy security requirements of the energy transition [1]. Fig. 1 represents a typical configuration of an AC Microgrid. Nowadays, research on MGs is still going on the integration of ESSs (Energy Storage Systems) with RESs is a promising approach to enhance the MG operation, energy quality and stability. ESSs are generally used in MG operation in order to assist RESs (Renewable Energy Sources) which have intermittent nature [2]. The combination of ESSs with RESs improves significantly the MG reliability, flexibility and power quality [3]. ESSs are vital in islanded MG in order to compensate the mismatch power between RESs and loads [4]. ESSs are also used for peak shaving, peak shifting, renewable smoothing, power quality improvement, congestion relief and other ancillary services [2], [5]. The most used type of ESSs in MG application are Batteries Energy Storage Systems (BESSs) thanks to their long-term application capability, fast dynamic response and energy absorption/release with acceptable cost [6], [7].

However, although the cost of BESS technologies has decreased significantly in recent years, their prices are still quite high at present [8]. Therefore, the efficient operation of BESSs becomes particularly important in order to avoid their fast degradation and also to extend their lifetime by considering their physical limitations (dynamics and SoC). Since SoCs in BESSs technologies are a crucial factor in checking whether the battery is in good condition, their SoCs must remain within a predefined range with respect to the battery technology. To ensure a better operation and therefore to extend the lifetime of BESSs, an operation range of 10%-90% or 20%-80% is commonly considered in literature. Generally, SoC synchronization methods [5], [8] are used in MG involving multiple DESSs units. DESSs SoC balancing control permits to avoid uneven degradation which greatly facilitates maintenance, to reduce the charge/discharge cycles that cause premature ageing and to extend BESSs lifetime by avoiding deep discharge and surcharge.

Extending BESSs lifetime has economic benefit since BESSs are still one of the costliest devices in the MG and great benefit for environment since BESSs are still not completely recyclable. SoC balancing has also the benefit to control DESSs ageing. SoC equalization can be achieved by using a centralized architecture controller [9], [10] or a distributed architecture controller [11]–[13], as represented in Fig. 2. A centralized architecture uses a MGCC (Microgrid Central Controller) to achieve the SoC synchronization by exchanging data with all DGs while a distributed architecture controller only exchanges information between DGs through a sparse communication network to ensure SoC synchronization. In distributed architecture, each DG as agent only receives information from its neighbors.

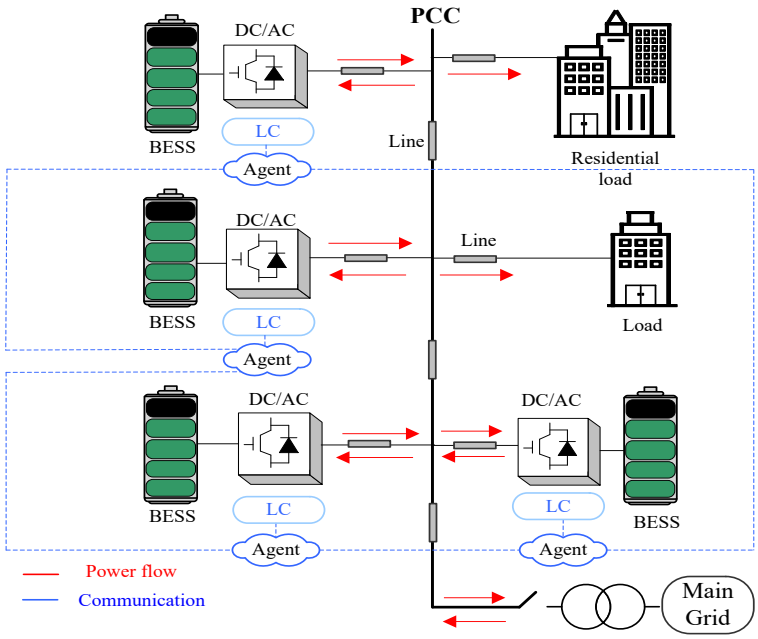

Fig. 1. Typical configuration for an AC Microgrid system with distributed control.

The main advantage of distributed controller is its robustness to communication failure. Unlike centralized control architecture which has a unique point of failure (MGCC default), the distributed architecture allows the continuity of system control when a communication failure happens and improves the system reliability and expandability.

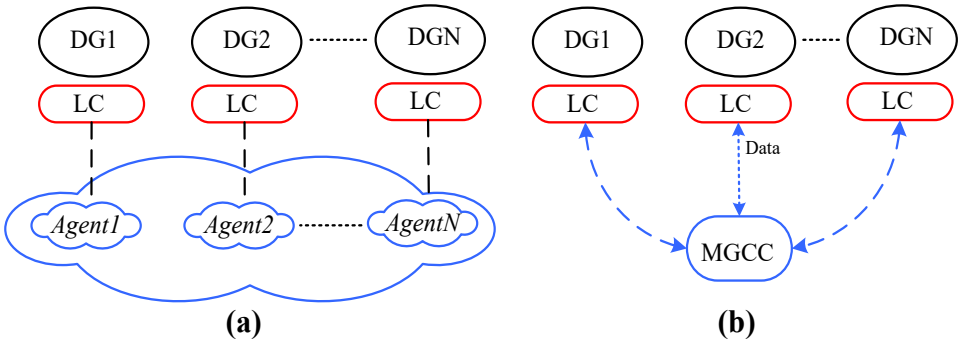

Fig. 2. (a): Distributed control architecture; (b): Centralized control architecture.

Many methods have been proposed in recent years to ensure DESSs SoC balancing. These methods are generally based on droop control with two different configurations that can be categorized as centralized and distributed methods. Reference [9] used a centralized control architecture to provide SoC balancing. Nevertheless, frequency and voltage restoration is not studied and a failure of the MGCC may result in the loss of SoC synchronization control. In [5], a multi-agent system (MAS) based on distributed control is used for SoC equalization without adding a control law (integrator). DGs frequencies are restored to their nominal values when SoC balancing is achieved, which may lead to a serious frequency deviation during the SoC balancing process if a sudden change in the MG system occurs, such as a large load variation. In addition, DGs voltage regulation is not studied in [5]. Authors of [8] achieved SoC balancing control in a distributed control architecture by introducing a PI controller into the P-ω droop control equation. In this control, the integral control is nullified when the errors between the SoCs of the DESSs become small. However, DGs frequency and voltage restoration is not investigated in this study. In [14] and [15], a distributed control-based MAS (Multi-Agent System) with consensus algorithm is used to achieve SoC equalization, frequency and voltage restoration thanks to an integral control. However, the SoC balancing control in charging mode is not studied in [15] since it is not performed by the secondary control but by the tertiary control. Reference [16] used a distributed control based on an adaptive frequency droop gain method to balance the SoC of the DESSs while ensuring frequency and voltage restoration. In this method,

using a PI controller, by changing the value of the frequency droop gain, the author can lead the DESS to provide more or less power to the MG. The restoration of the frequency and voltage is performed in [16]. However, modifying the gain of the P-ω droop equation to ensure SoC synchronization can result in stability issues. An adaptive virtual resistance method is used in [17] to balance the discharge rate of BESSs through a PID controller in a distributed architecture. By adjusting the virtual resistance, this control balances the SoC of BESSs that have different capacities. However, the voltage and frequency restoration of the MG is not studied. In [18], an adaptive frequency droop based on virtual power is implemented to ensure SoC balancing by introducing a virtual power in the P-ω droop equation in a distributed control-based MAS. The virtual power used for SoC balancing is calculated by means of a PI controller. Frequency and voltage restoration is also achieved in [18]. A distributed terminal sliding mode controller is used for robust SoC balancing control in [19] using an integral control. DGs frequency and voltage are restored to their nominal values.

In most all the strategies presented above except for the method used in [5], an integral control is introduced for each DESS in order to ensure SoC synchronization and frequency restoration. These controls increase the system order and have a constraining bandwidth that can bring stability problems. Sizing the control parameters of such controls becomes a difficult problem since oversized parameters introduce interaction with the internal loops that leads to instability and undersized parameters lead to poor performance. The problem of sizing the control parameters becomes more challenging, especially when the number of DESS is high or increases with the expansion of the microgrid. The few methods in which an integrator is not added generally result in poor performance of the SoC synchronization strategy and frequency restoration, with the inability to eliminate static error. Therefore, a method to get rid of the integral control while ensuring high control performance for SoC synchronization and frequency restoration is needed.

In this paper, a new resilient distributed control is used for an effective power management in an AC islanded microgrid based on DESSs. The proposal achieves SoC balancing and frequency restoration with high resilience under constraining operating conditions (communication failure, communication delay or loads/sources impacts) and with high performance without introducing a local integral control. Beyond the power quality aspects, such a management will allow a better exploitation of the distributed storage units, leading to a better lifespan of these elements. Functionally, the design of the secondary management algorithm uses active power references that are sent to the primary level to achieve SoC synchronization. Each DESS provides active power to the MG based on its participation level which is determined through a modified dynamic average consensus. In addition, the active power references are chosen to stabilize the DGs frequency at the nominal frequency of the MG. Thus, the DG frequency is instantly restored to its nominal value without waiting for the SoC synchronization and this without any additional control for the frequency restoration. Only voltage restoration control is implemented.

SoC balancing, frequency regulation as well as voltage regulation are achieved in a fully distributed architecture controller where three information (errors on average active power, errors on average SoC and voltage) are exchanged between the DGs through a sparse communication network. The main contributions of this proposal are as follows:

1) A novel SoC balancing technique that achieves accurate power sharing without using additional control laws as commonly done in the literature, and operating perfectly in charging and discharging mode is proposed.

2) Frequency regulation is automatically achieved in this proposal without using additional control laws, since the secondary control provides to the primary levels, the appropriate active power reference that set the DG frequency to the nominal value.

3) Moreover, the distributed control ensures high resilient and performance under constraining operating conditions such as a partial communication loss, communication time delay and a suddenly connection or disconnection of a DG unit or loads.

4) In addition, the SoC balancing and frequency restoration control parameters are easy to design and depend only slightly on the system parameters. Therefore, there is no need to resize the control parameters when expanding the MG as long as the same communication topology is maintained.

5) Compared to the methods in the literature where a P or PI or PID controller is used, in the proposed strategy, no power is shared between the DESSs at zero load and RESs power. Hence, the losses and aging of the batteries are reduced when no load is connected to the MG.

The rest of the paper is organized as follows: In Section 2, the studied system is presented. The proposed method for SoC balancing and voltage regulation is investigated in Section 3. Simulation results are presented in Section 4 and experimental results in Section 5. Section 6 concludes this paper.

2. Studied system description

2. 1. Studied system

The general synoptic scheme of the studied system for this proposal is presented in Fig. 3. This System represents a case of an AC Microgrid with DG units based on batteries that supply local loads. The DGs are interconnected through lines and each load is connected to a local point of common coupling.

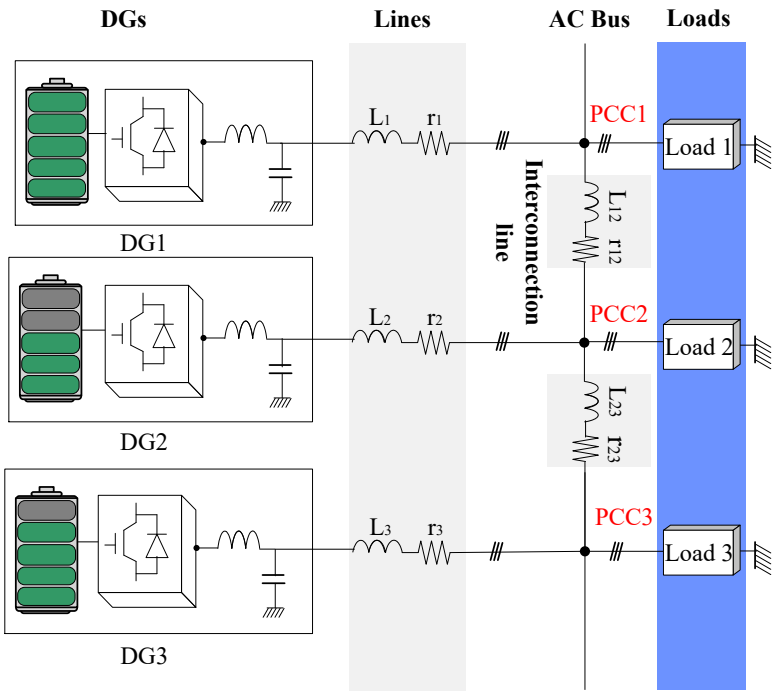

Fig. 3. Studied System: MG based on 03 DESSs supplying 03 loads

2. 2. BESSs SoC estimation method

Many strategies have been developed in the literature [20]–[22] to estimate the states of charge of the BESSs units. Since this paper only interest is the BESSs SoC synchronization, the coulomb counting method in [6] is used for the BESSs SoC estimation and can be described as follows:

$$SoC_i = SoC_{init} - \frac{1}{C_i}\int I_i dt \tag{1}$$

with SoC_{init} represents the initial SoC of the $BESS_i$; C_i denotes nominal capacity of the $BESS_i$ and I_i is the output current of the $BESS_i$.

By omitting the BESS power loss, the real power of the BESS can be expressed as:

$$P_i = V_i I_i => I_i = \frac{P_i}{V_i} \tag{2}$$

By combining (1) and (2), the SoC estimation can be expressed as:

$$SoC_i = SoC_{init} - \frac{1}{\mu_i}\int P_i dt \tag{3}$$

$$\mu_i = C_i V_i \tag{4}$$

where P_i, V_i denotes the BESS active power and output voltage respectively.

In the next section, the proposed strategy for SoC equalization is explained.

3. Proposed distributed control for SoC balancing and voltage regulation

Distributed control is recently widely used in MG especially for secondary control. It is a promising approach to enhance islanded MG reliability, stability and performance [23]. Many works have been already proposed to ensure distributed secondary control [11]–[13]. Distributed control has many advantages such as reduction of the communication infrastructure cost, reduction of computational burden, more reliable and adapted for large and complex MG compare to centralized control.

In this section, an enhance fully distributed control architecture is proposed for DESSs SoC synchronization and voltage/frequency restoration.

3. 1. Graph theory and distributed control based on consensus

Distributed control communication network can be expressed by a graph G= (V, E), with V $= \{v_1, v_2, \dots, v_N\}$, the set of N nodes or N agents and E$\subseteq V \times V$, the set of edges or arcs. Elements of E are denoted as (v_i, v_j) and represent the arcs from node v_i to node v_j and are represented with arrows at unique or double direction depending on the information flow between the two nodes (unidirectional or bidirectional) as illustrated in Fig. 4.

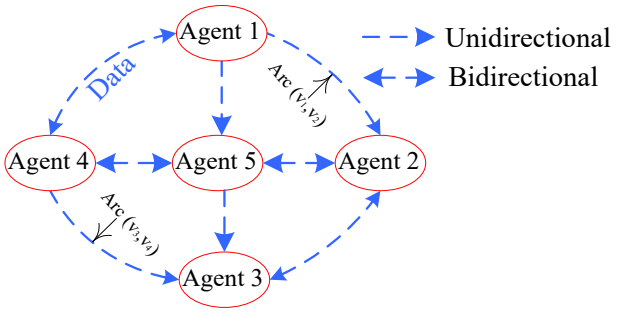

Fig. 4. Representative graph with five agents.

Each edge (v_i, v_j) is associated with a weight a_{ij}>0 if v_i receives information from v_j else $a_{ij} = 0$. The adjacency matrix is defined as: A=$[a_{ij}]$ and the graph Laplacian matrix as *L=D-A*. D is the diagonal matrix defined as: *D=diag*$\{d_i\}$ and d_i=$\sum_{j=1}^{N} a_{ij}$.

In order to bring all the agents to converge to the same value, the distributed control-based consensus protocol is defined as [23]:

$$\mu_i = \sum_{j=1}^{N} a_{ij}\left(x_j - x_i\right) + b_i(x_i - x_0) \tag{5}$$

where b_i>0 if the agent v_i has the information about the consensus value, otherwise $b_i = 0$.

With this protocol, the global dynamic protocol can be defined as:

$$\dot{X} = K\left(-LX + B(X_0 - X)\right) \tag{6}$$

where $X = [x_1, \dots, x_N]'$; $X_0 = [x_{01}, \dots, x_{0N}]'$; B=diag$\{b_i\}$,the diagonal pinning matrix; $L = D - A$, the Laplacian matrix and K, the consensus gain.

For the studied system defined in Fig. 3 with three DESSs (three agents), the adjacency matrix *A*, the Laplacian matrix *L* and the pinning matrix B are defined respectively as:

$$A=\begin{pmatrix}0 & 1 & 1\\ 1 & 0 & 1\\ 1 & 1 & 0\end{pmatrix}, L=\begin{pmatrix}2 & -1 & -1\\ -1 & 2 & -1\\ -1 & -1 & 2\end{pmatrix}; \text{B}=\begin{pmatrix}1 & 0 & 0\\ 0 & 0 & 0\\ 0 & 0 & 0\end{pmatrix}$$

3. 2. DESSs SoC balancing and voltage regulation

Conventionally, droop control is used for power sharing in the MG. This control brings all DGs to provide powers according to their nominal powers. The droop control equations are represented as follows [24]:

$$\omega_i = \omega_n - m_i(P_i - P_{in}) \tag{7}$$

$$V_i = V_n - n_i(Q_i - Q_{in}) \tag{8}$$

with $\omega_n, V_n, m_i = \frac{\Delta\omega}{P_{in}}, n_i = \frac{\Delta V}{Q_{in}}, P_i, Q_i, P_{in}, Q_{in}$ are respectively the MG nominal frequency, the MG nominal voltage, the frequency droop coefficient, the voltage droop coefficient, the DG_i active power, the DG_i reactive power, the nominal DG_i active power and the DG_i nominal reactive power. $\Delta\omega$ and ΔV represent maximum deviation of the frequency and voltage respectively.

This type of strategy is not well suited for a MG with DESSs because a battery with a lower state of charge would provide more power than another one that has a higher SoC in discharging mode resulting deep discharges issues.

The main idea of SoC synchronization strategy is to make sure that the battery with the highest (respectively the lowest) SoC provides more (respectively less) power in discharging mode. In charging mode, this strategy ensures that the battery with the highest (respectively the lowest) state of charge, receives less (respectively more) power.

In this paper a new strategy is proposed for DESSs SoC balancing. The global dynamic equation of the proposed method to ensure the DESS SoC equalization is reported in the equation (9). In order to fill the requirements, set above for SoC synchronization, active power references are used for SoC balancing. These active power references (P_{iref}) are calculated as shown in equation (10) thanks to the level of participation (K_{iSoC}) of the DESS that depends on the state of charge and is evaluated in equation (11).

$$\omega_i = \omega_n - m_i(P_i - \boldsymbol{P_{iref}}) \tag{9}$$

$$P_{iref} = \boldsymbol{K_{iSoC}P_{it}} \tag{10}$$

$$K_{iSoC} = \frac{\boldsymbol{SoC_{im}}}{\boldsymbol{SoC_{imt}}} \tag{11}$$

$0 < K_{iSoC} < 1$ and $\sum_{i=1}^{N} K_{iSoC} = 1$ and $\sum_{i=1}^{N} \boldsymbol{P_{iref}} = \boldsymbol{P_{it}}$

with $\boldsymbol{P_{it}}$**:** DESSs total active power and $\boldsymbol{K_{iSoC}}$**:** level of participation of the $DESS_i$.

$\boldsymbol{SoC_{im}}$ and $\boldsymbol{SoC_{imt}}$ represent respectively the modified SoC_i of the $DESS_i$ and the total modified SoC_i of all DESSs and are evaluated in the equation (12) and (13).

$$SoC_{im} = \boldsymbol{\alpha_{SoC}} \boldsymbol{SoC_i}^{k\sigma_i} \tag{12}$$

$$SoC_{imt} = \sum_{i=1}^{N} SoC_{im} \tag{13}$$

N is the number of DESSs in the MG.

$k \geq 1$ represents the SoC balancing convergence speed coefficient. The greater is k, the faster the batteries SoC converge toward the same value.

$\boldsymbol{\sigma_i = -1}$ in charging mode and **1** in discharging mode.

In order to evaluate SoC_{imt} and P_{it} in a distributed way, the proposed modified dynamic average consensus in [5] is used (refer equation (15) and (16)). The SoC balancing coefficient $\boldsymbol{\alpha_{SoC}}$ (equation (14)) is introduced in the equation (12) to make sure that the modified dynamic average consensus converges in discharging and charging mode by keeping SoC_{imt} around the same magnitude in charging and discharging mode.

$$\alpha_{SoC} = 10^{-\delta\sigma_i} \tag{14}$$

$$X_{it}[l+1] = N(X_i[l] + \lambda_{mean} \sum_{\substack{j \in N_i \\ j \neq i}} \beta_{ij}[l+1]) \tag{15}$$

$$\beta_{ij}[l+1] = \beta_{ij}[l] + X_{jmean}[l] - X_{imean}[l] \; (i \neq j) \tag{16}$$

where δ represents a coefficient that depends on the SoC balancing convergence speed coefficient (k) and should be chosen to keep SoC_{imt} around the same magnitude in charging and discharging mode; l represents the iteration; X_{it} can be replaced in our case of study by SoC_{imt} and P_{it}; λ_{mean}: modified average consensus gain and is set based on the convergence speed of the consensus algorithm and stability in general [5].

From the point of view of frequency and voltage stabilization services, the proposed secondary control strategy for the DESSs allows:

- A stabilization of the frequency is achieved automatically in the investigated system, since the secondary control provides to the primary levels the appropriate active power references ($P_i = P_{iref}$) that stabilizes the frequency at its nominal value f_n. Therefore, either in the presence of sudden load changes, the control enables fast disturbance rejection with reduced impact on the frequency.
- Regulation of the DGs voltage is achieved by means of a consensus control which principle is detailed above in equation (5).

Equations for the distributed control-based consensus for voltage restoration are designed as follows:

$$\dot{X}_v = K_v\left(-L\bar{V} + B(\bar{V_n} - \bar{V})\right) \tag{17}$$

with $X_v = \begin{pmatrix} x_{1v} \\ x_{2v} \\ x_{3v} \end{pmatrix}; \bar{V} = \begin{pmatrix} V_1 \\ V_2 \\ V_3 \end{pmatrix}; \bar{V_n} = \begin{pmatrix} V_n \\ V_n \\ V_n \end{pmatrix};$

with K_v: voltage consensus control gain; L: Laplacian matrix; B: diagonal pinning Matrix and x_{iv} the voltage compensator of the $DESS_i$.

The dynamic equation for voltage control is represented in equation (18). The global control scheme for SoC balancing and for voltage regulation for a DG unit is reported in Fig. 5.

$$V_i = V_n - n_i(Q_i - Q_{in}) + \boldsymbol{x_{iv}} \tag{18}$$

3. 3. Design of the control parameters

This section is dedicated to the design of the control parameters k, δ and λ_{mean}.

The first parameter to choose is the SoC balancing coefficient (k) which will determine the convergence speed of the battery SoCs to the same value. The higher k is, the faster the batteries will converge to the same state of charge. A k=5 gives very good results in terms of convergence

speed of the SoC balancing but the k can be chosen larger as long as the computing device manages to calculate the SoC_{im}.

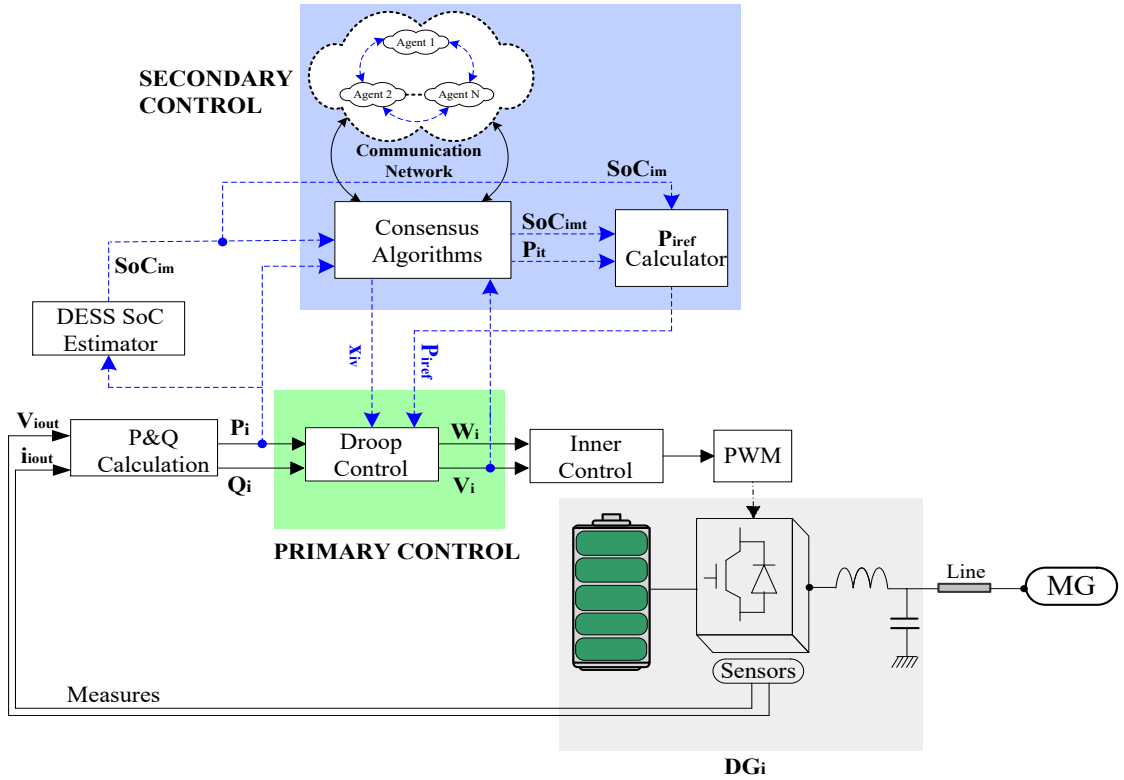

Fig. 5. Global control scheme for a DG_i.

The proposed control scheme automatically avoids charging one battery while discharging another, because K_{iSoC} is always less than 1, regardless of the value of k, there will never be a risk of one battery discharging to charge another in order to ensure the SoCs balancing. The maximum value of k will therefore be limited by the capacities of the computer.

The second parameter to choose is the consensus coefficient δ which depends on k. The role of this coefficient is to keep the value of SoC_{im} at the same order of magnitude in charging and discharging mode thanks to the coefficient α_{SoC}. In fact, in charging mode, the values of SoC_{im} become very small while in discharging mode, their values become larger. Therefore, this will make the convergence of the modified average consensus algorithm for the same parameter λ_{mean} complex. To avoid the divergence of the consensus algorithm for the evaluation of SoC_{imt}, the coefficient δ should be well chosen to allow the convergence of the algorithm in both modes

of operation, by reducing the value of SoC_{im} in discharging mode and increasing it in charging mode.

Example: Assuming that the SoCs of the DESSs are limited between 20 and 90% to avoid deep discharges and overloads. For a $\boldsymbol{k}$ =6, we have the following:

maximum value of SoC_{im} in charging mode: $20^{-6} = 1.5625\text{e-}08$ (very small);

maximum value of SoC_{im} in discharging mode: $90^{6} = 5.3144\text{e+}11$ (very high).

It can be seen that there is a very large difference between the maximum value of the SoC_{im} in charging mode and in discharging mode. This will lead to the divergence of the consensus algorithm in charging mode, hence the need to apply the coefficient α_{SoC}.

After applying the coefficient α_{SoC} with a δ=9:

maximum value of SoC_{im} in charging mode: $10^{9} * 20^{-6} = 15.625$;

maximum value of SoC_{im} in discharging mode: $10^{-9} * 90^{6} = 53.144$.

With a δ =9, we make sure that the SoC_{im} values remain close both in charging and discharging mode to ensure the convergence of the algorithm for the determination of the SoC_{imt}.

The last and most important parameter to set is the consensus gain (λ_{mean}). λ_{mean} depends on the chosen magnitude of the SoC_{im} and the topology of the communication network between the agents. λ_{mean} is set based on the convergence speed of the consensus algorithm and its stability. The value of λ_{mean} must be chosen small enough to allow the convergence of the algorithm. As it is shown in [5], a large value of the consensus gain increases the convergence speed of the algorithm, but can also lead to its instability if the selected the consensus gain is too large.

It can be seen that the parameters of the proposed control depend much more on the topology of the communication network than on the parameters of the MG system. Therefore, a redesign of the proposed control parameters is not necessary when the size of the MG increases as long as we keep the same communication topology for the agents.

4. Simulation results

To investigate the proposed strategy for DESSs SoC synchronization, a MATLAB/Simulink simulation is performed on the studied system reported in Fig. 3. The MG System parameters are reported in Table 1. Four tests are realized in this section. First test, to validate the SoC balancing method in discharging mode. Second test, to validate the proposed method for SoC balancing in charging mode. Third test, to investigate the impact of communication failure on this strategy and the final test for the plug and play capability. In all tests, the load 3 is disconnected at 300 s and reconnected at 600 s.

Table 1

System parameters.

Item	Symbol	Value
MG Parameters		
Line impedance DG1	r_1, L_1	0.1Ω, 1mH
Line impedance DG2	r_2, L_2	0.1Ω, 0.6mH
Line impedance DG3	r_3, L_3	0.1Ω, 1mH
Line impedance DG1-2	r_{12}, L_{12}	0.1Ω, 0.6mH
Line impedance DG2-3	r_{23}, L_{23}	0.1Ω, 0.6mH
Rated powers DG1	P_{1n}, Q_{1n}	1500 W, 1500 VAR
Rated powers DG2	P_{2n}, Q_{2n}	2000 W, 1000 VAR
Rated powers DG3	P_{3n}, Q_{3n}	2500 W, 500 VAR
Load 1, 2, 3	R_{ch}	52 Ω
MG frequency/voltage	f_n/V_n	60Hz/110V
Constant for SoC estimation	μ_i	$2500(\mathrm{Ah.V})^{-1}$
Control Parameters		
Max f & V deviation	Δ_f/Δ_V	0.5 Hz/5V
SoC balancing coefficient	k	5
Consensus coefficient	δ	8
Consensus gain	λ_{mean}	0.1
Voltage Consensus gain	K_v	5

4. 1. Test 1: SoC balancing in discharging mode

First test is dedicated to show the effectiveness of the proposed method for DESSs SoC balancing in discharging mode. Initially, the DESS 1, 2 and 3 states of charge are respectively set to 100, 93 and 85%. Simulation results are represented in Fig. 6. The states of charge of the DESSs are presented in Fig 6 (a), DESSs frequency and voltage (f & V) variations are represented in Fig. 6 (b) and Fig. 6 (c) respectively. Active powers of the DESSs are reported in Fig. 6 (d). Fig 6 (a) shows that the SoCs of all DESSs converge toward the same value and are well synchronized at 600s. Since all BESSs have the same capacity, their active powers also converge toward the same value as presented in Fig 6 (d).

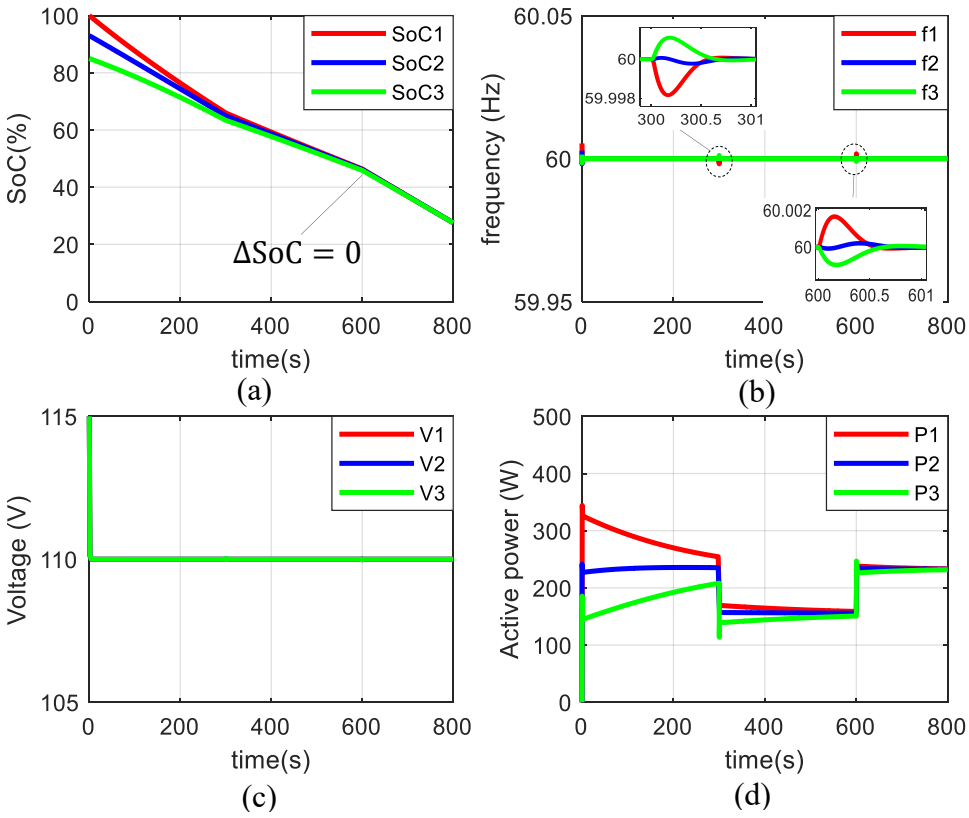

Fig. 6. SoC balancing under discharging mode with a load impact at 300 and 600s: (a) SoC behavior of the 03 batteries; (b), (c) and (d) measured frequency, RMS voltage and active power at the output of the 03 DGs units.

Despite the load variation at 300s and 600s the frequency and voltage of the DESSs remain to their nominal values (Fig 6 (b) and (c)) during the MG operation. Even if small peaks of the f

& V are observed under load change it remains negligible and the f & V are restored to their nominal values within 1s.

4. 2. Test 2: SoC balancing in presence of variable renewable energy power

Second test is realized to verify the effectiveness of the SoC synchronization method in charging mode and the performance of the proposed scheme in presence of variable renewable energy power. An active power profile shown in Fig. 7 (a) and imitating RESs (PV and WT) power generation is injected in the MG.

DESS 1, 2 and 3 SoCs are initially set to 50, 45 and 40% respectively. Simulation results are represented in Fig. 7. The states of charge of the DESSs are presented in Fig 7 (b). It can be seen that between 0h00min and 6h15min, the DESSs are in discharging mode because the power of the RESs is lower than the power of the loads. The DESS 1 which has the highest SoC provides the highest power to the MG (Fig. 7 (c)). However, at 6h15min, when the power of the RESs becomes higher than the power of the loads, the DESSs switch to charging mode and this time, the DESS 3 which has the lowest SoC that receives the most active power (Fig. 7 (c)), thus resulting in an equalization of the SoCs at 12h30min (Fig 7 (b)). The proposed control ensures SoC balancing, despite the injection of variable power from renewable energy sources. DGs frequency and voltage variations are reported in Fig. 7 (d) and Fig. 7 (e) respectively and remain to their nominal values in spite of the load and RESs power variations. Also note that slight frequency and voltage variations occur during disconnection and reconnection of load 3, but they remain negligible.

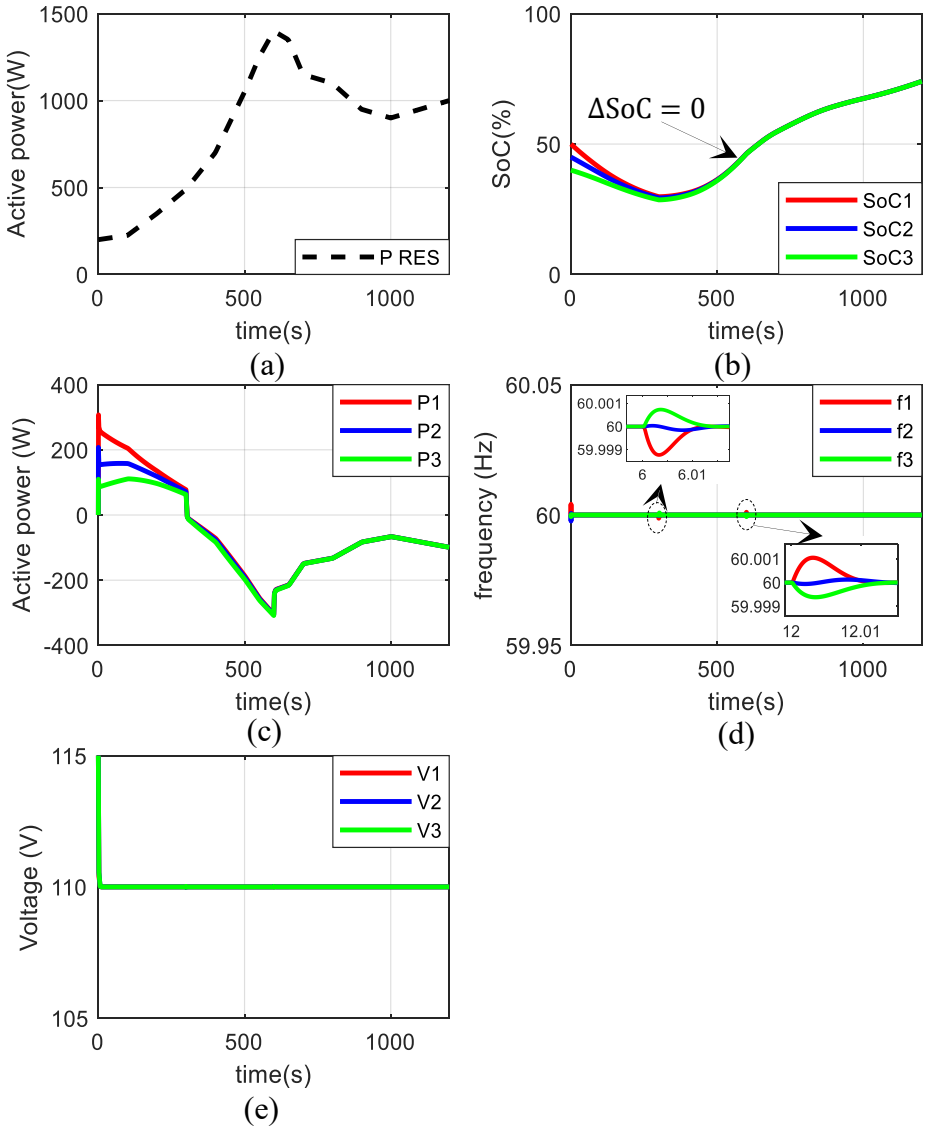

Fig. 7. SoC balancing in charging mode with injection of variable renewable energy power and load impact at 6h and 12h: (a) RESs active power (b) SoC behavior of the 03 BESSs; (c), (d) and (e) measured active power, frequency and RMS voltage at the output of the 03 DGs units.

4. 3. Test 3: Communication Failure

The third test is dedicated to the robustness of the proposed SoC balancing method against communication failure. In order to see the impact of communication failure of the proposed method, a communication link failure between the agent 1 and 2 is initially simulated as

reported in Fig. 8. The two agents can no more exchange and information to each other ($\boldsymbol{a_{12} = 0, a_{21} = 0}$).

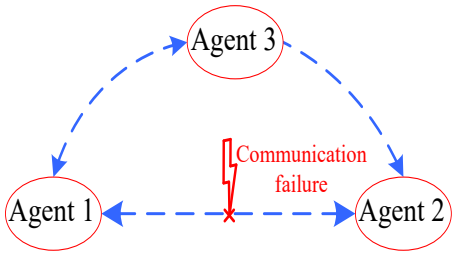

Fig. 8. Communication network with a failure between agent 1 and 2.

For this test, the DESS 1, 2 and 3 SoC are initially set to 100, 93 and 85 % respectively. Results are represented in Fig. 9. The SoCs of the DESSs are presented in Fig 9 (a), frequency and voltage of the DESSs are represented in Fig. 9 (b) and Fig. 9 (c) respectively. Active powers of the DESSs are reported in Fig. 9 (d).

Results in Fig 9 (a) show that despite the loss of communication between the two agents 1 and 2, the SoCs of all DESSs are well balance to the same value at 600s. Communication failure between two agents has so no impact on the performance the proposed SoC balancing method. It can be seen that the frequency and voltage of the DESSs remain to their nominal (Fig 9 (b) and (c)) values during the MG operation. Voltage regulation control is not affected by the loss of the communication link.

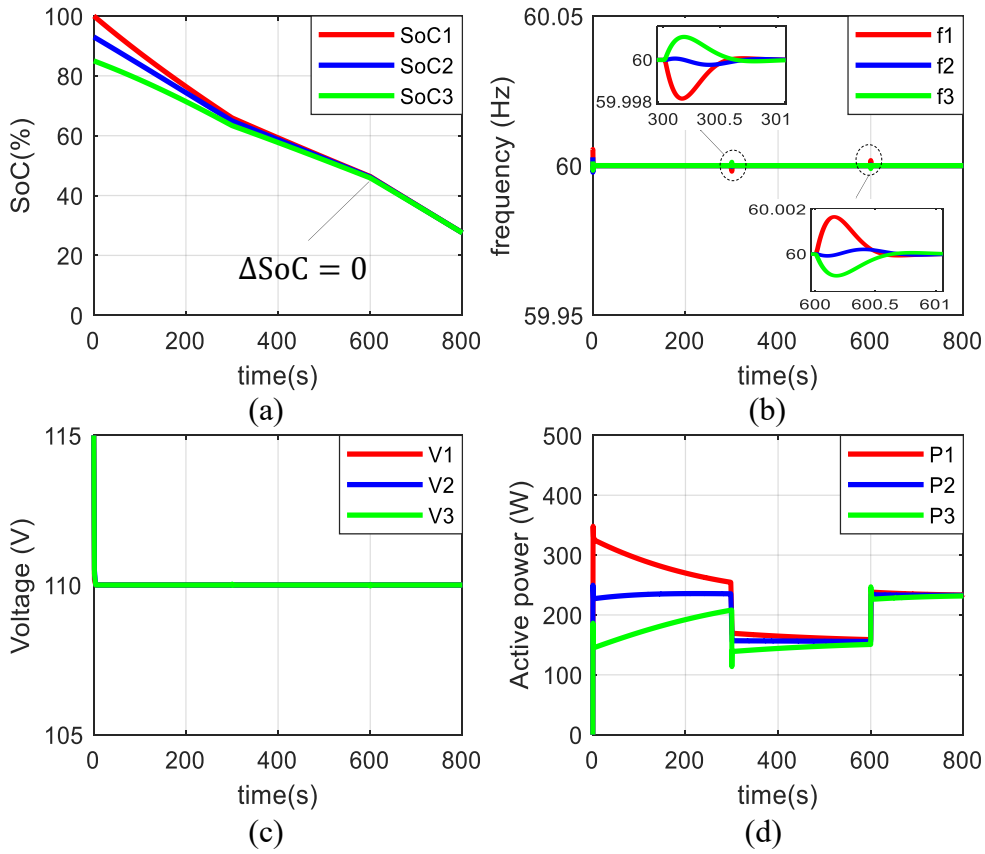

Fig. 9. SoC balancing under communication failure with a load impact at 300 and 600s: (a) SoC behavior of the 03 batteries; (b), (c) and (d) measured frequency, RMS voltage and active power at the output of the 03 DGs units.

4. 4. Test 4: Plug and play

In the fourth test, the SoC of the DESS 1, 2 and 3 are respectively set to 100, 95 and 90%. In order to investigate the "Plug and Play" capability, the DESS 3 is disconnected at t=350s and reconnected at t=430s. Simulation results are represented in Fig. 10. The states of charge of the DESSs are presented in Fig. 10 (a), frequency and voltage of the DESSs are represented in Fig. 10 (b) and Fig. 10 (c) respectively. Active powers of the DESSs are reported in Fig. 10 (d).

Between 0 and 350s all DGs are connected to the grid. SoCs of the DESSs converge to the same value (Fig. 10(a)) and the DESSs provide powers according to their SoCs. However, at t=350s, the DESS 3 is disconnected. DESS 3 shares no active power $P_3 = 0$ (Fig. 10 (d)) and

the DESS 3 SoC remains to 63%. SoC balancing is ensured only between the DESS 1 and 2 until the DESS 3 is reconnected at 430s. Then, the DESS 3 supplies power to the MG. The SoC of the DESS 3 converges toward the same value as DESS 1 and 2 resulting the synchronization of their SoCs (Fig. 10 (a)) at t=787s. It is also worth mentioning that DGs voltage and frequency (Fig. 10 (b) and Fig. 10 (c) respectively) remain to their nominal values after a disconnection or connection of the DESS 3 though small peaks are perceived.

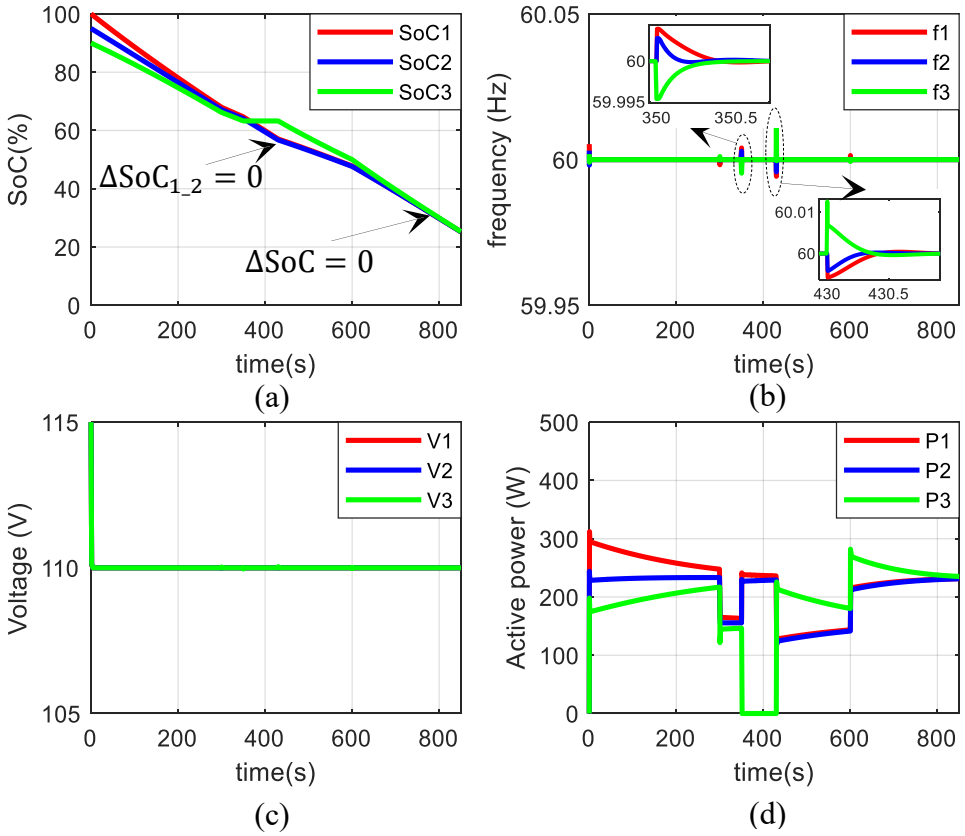

Fig. 10. SoC balancing under "plug and play" condition with a load impact at 300 and 600s: (a) SoC behavior of the 03 batteries; (b), (c) and (d) measured frequency, RMS voltage and active power at the output of the 03 DGs units.

4. 5. Test 5: Communication delay

Since the proposed method relies on a communication network to exchange information, there is usually a time delay in the sparse communication network. A latency in the range of 0.3s to 2s is generally observed for the control of distributed energy resources in a MG [25]. By

considering the worst-case scenario, the impact of a 2 s constant time delay on the proposed method (SoC balancing and voltage regulation) is analyzed in this test using a first-order rational polynomial approximation. Simulation results are represented in Fig. 11. The states of charge of the DESSs are presented in Fig. 11 (a), frequency and voltage of the DESSs are represented in Fig. 11 (b) and Fig. 11 (c) respectively. Active powers of the DESSs are reported in Fig. 11 (d).

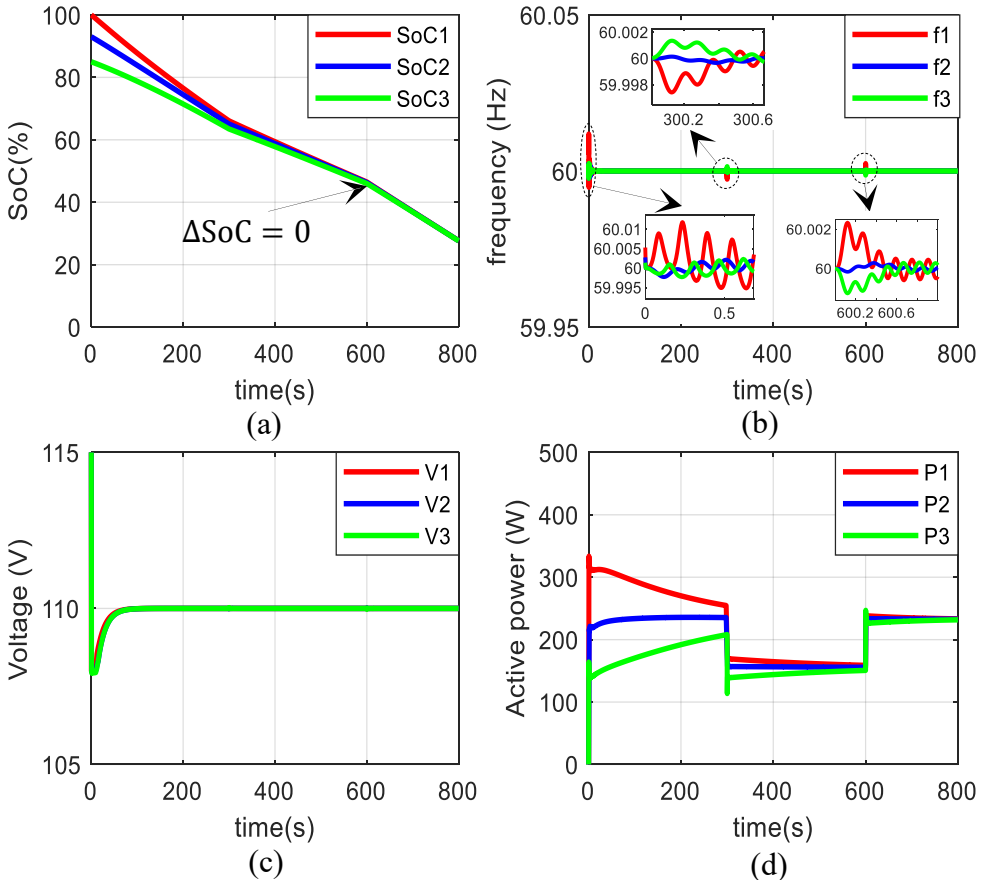

Fig. 11. SoC balancing with 2s time delay: (a) SoC behavior of the 03 batteries; (b), (c) and (d) measured frequency, RMS voltage and active power at the output of the 03 DGs units.

As it can be seen in Fig. 11 (b) and Fig. 11 (c), at start-up the restoration of the voltage and frequency of the DGs to their nominal values takes longer (83s for the voltage and 10s for the frequency) because of the 2s delay time implemented in the communication network. After the startup, the DGs frequencies and voltages are regulated to their nominal values and the MG remains stable despite the load variation at 300s and 600s. All DESSs achieve SoC balancing at

600 s as illustrated in Fig. 11 (a). The SoC balancing convergence speed is almost unaffected by the time delay. The proposed method achieves SoC balancing despite the communication network having a time delay and a 2 s time delay has almost no effect on the dynamic convergence characteristics of the SoC.

4. 6. Test 6: Comparison with other method

A comparison with the SoC balancing technique used in [18], where local integral control is introduced, is performed to evaluate the performance of the proposed scheme. All loads are disconnected at t=50s and then reconnected at t=500s in both controls. The obtained results are shown in Fig. 12. Results of the proposal are represented to the left and obtained results with the method used in [18] are represented to the right. It can be seen in Fig. 12 (b) that SoC balancing is achieved between 50s and 500s in the control using an integral despite the zero-load power. Indeed, to ensure the balancing of the SoC, the DESS 1 discharges to recharge the DESS 2 and 3 (Fig. 12 (d)). This leads to unnecessary losses in the MG which should be avoided. While, in the proposed method, as can be seen in Fig. 12 (a), at no load power between 50s and 500s, no power is exchanged between the DESSs (Fig. 12 (c)) and their SoCs remain constant. The SoC balancing is ensured after the reconnection of the loads to the MG (Fig. 12 (a)). The proposed control method therefore prevents a battery from discharging in order to charge another one and as a result reduces the losses at zero load power contrary to the methods used in the literature.

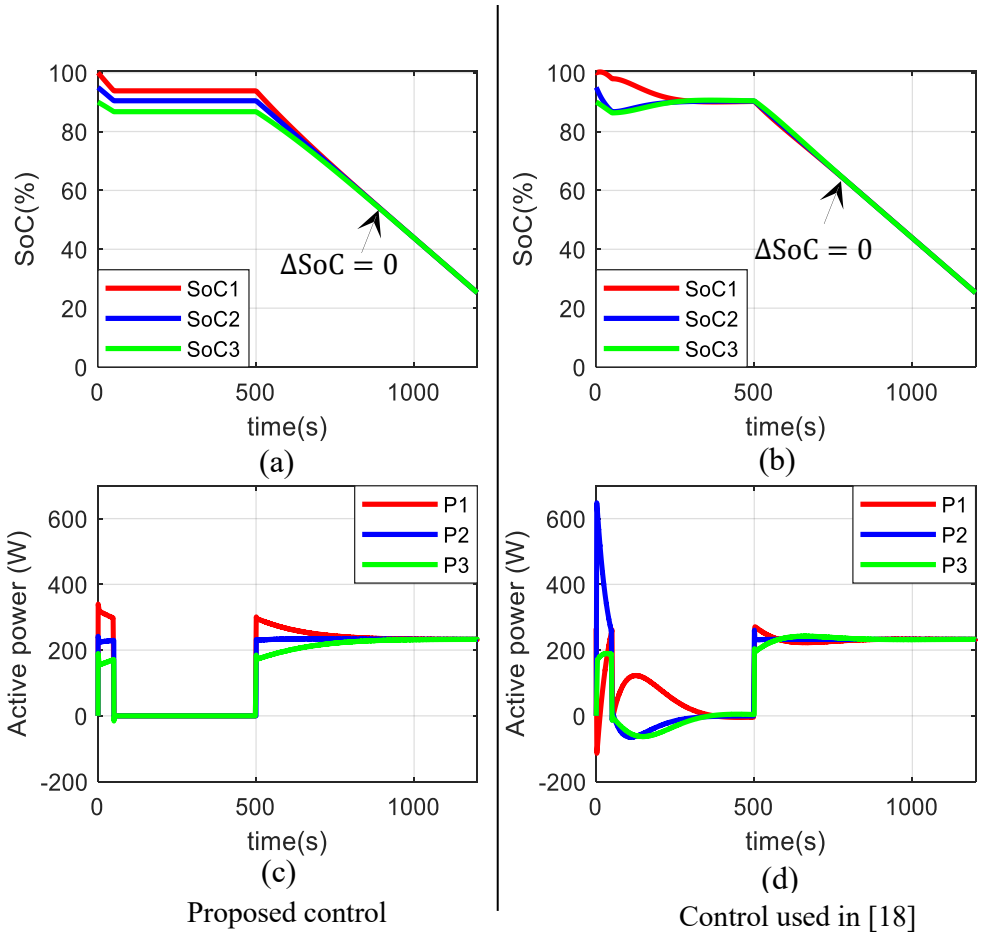

Fig. 12. Comparison between the proposed control and the control used in *[5]*: (a) SoC behavior of the 03 batteries; (b), (c) and (d) measured frequency, RMS voltage and active power at the output of the 03 DGs units.

5. Experimental results

In order to verify the effectiveness of the proposed method for DESSs SoC balancing, experimental tests in different case scenario are performed on the experimental setup reported in Fig. 13. The setup consists of a cinergia GE & EL-20 used in AC Grid Emulator (GE), a dSPACE JUIL-2010 system with a controldesk, a three-phase resistive load, two three-phase inductances (one for DESS unit line and the another one for interconnection line) and a switch to simulate a loss of a DESS unit. Each AC phase of the cinergia can be controlled independently and represents a DESS unit. The three single-phase DGs units are relied to an AC bus through lines and interconnection lines. Each local Point of Common Coupling (PCC) supplies a local resistive load. The experimental setup configuration scheme is represented in

Fig. 14. Each DESS unit is modeled in the dSPACE as discussed in 2. 2. The proposed control algorithm is implemented and compiled from Simulink to dSPACE to control each DESS unit of the GE. Four tests are realized in this section: First test to validate the SoC balancing method. Second test to investigate the proposed method under loads change. Third test to investigate the impact of communication failure on the proposal. Fourth test to investigate the plug and play capability.

In all four tests, the DESS 1, 2 and 3 SoC are initially set to 100, 95 and 90% respectively. The experimental setup parameters and control parameters are reported in Table 1.

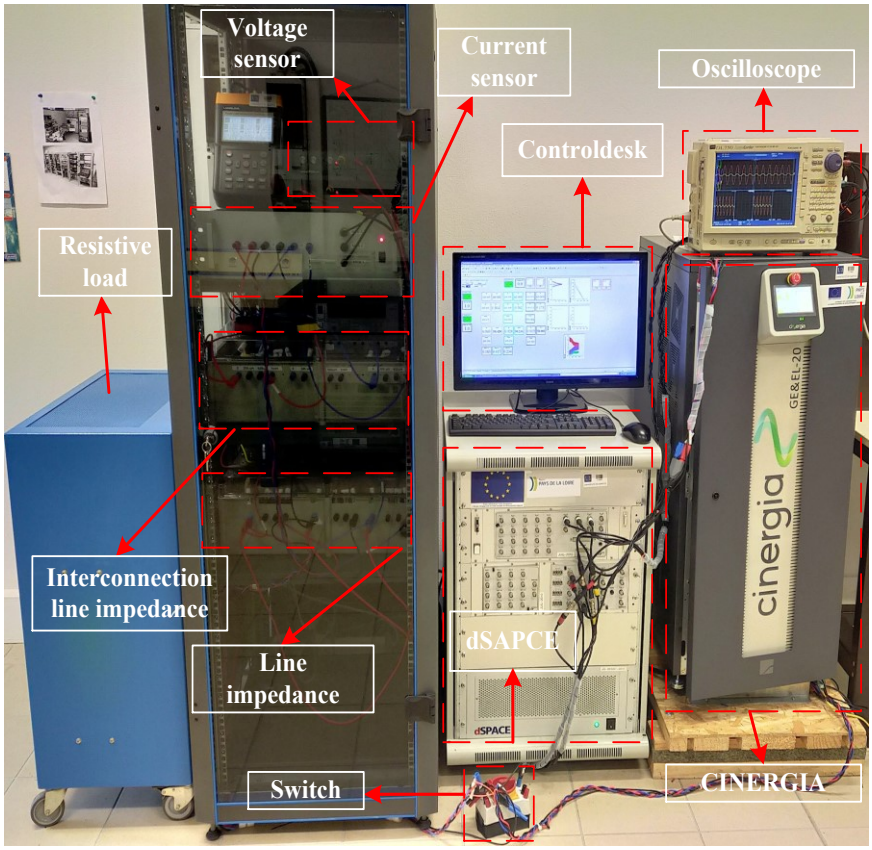

Fig. 13. Experimental setup.

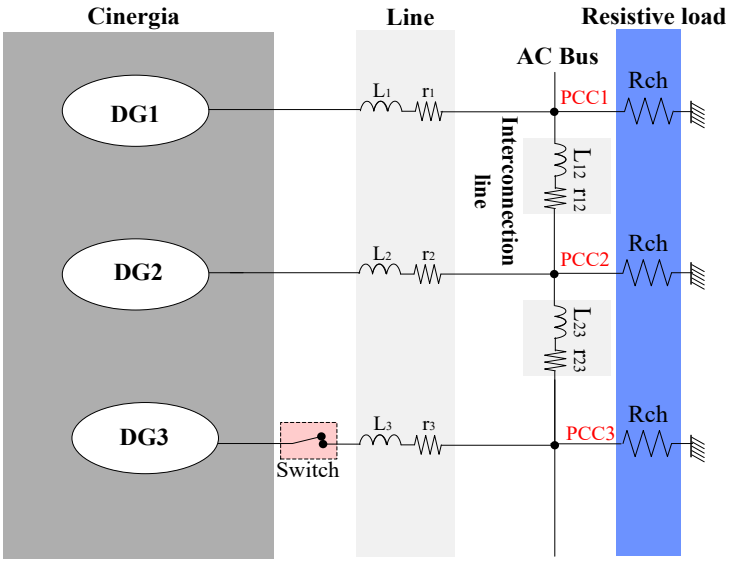

Fig. 14. System configuration scheme.

5. 1. Test 1: SoC balancing verification

First test is dedicated to show the effectiveness of the proposed method. Experimental results are represented in Fig. 15. The states of charge of the DESSs are presented in Fig. 15 (a), DESSs voltage and frequency variations are represented in Fig. 15 (b) and Fig. 15 (c) respectively. Active powers of the DESSs are reported in Fig. 15 (d).

Fig. 15 (b) shows that each DESS supplies power to the grid according to its SoC resulting a SoC synchronization at 494 s as shown in Fig. 15 (a). As expected, frequency and voltage of the DESSs remained to their nominal (Fig. 15 (b) and (c)) values during the MG operation.

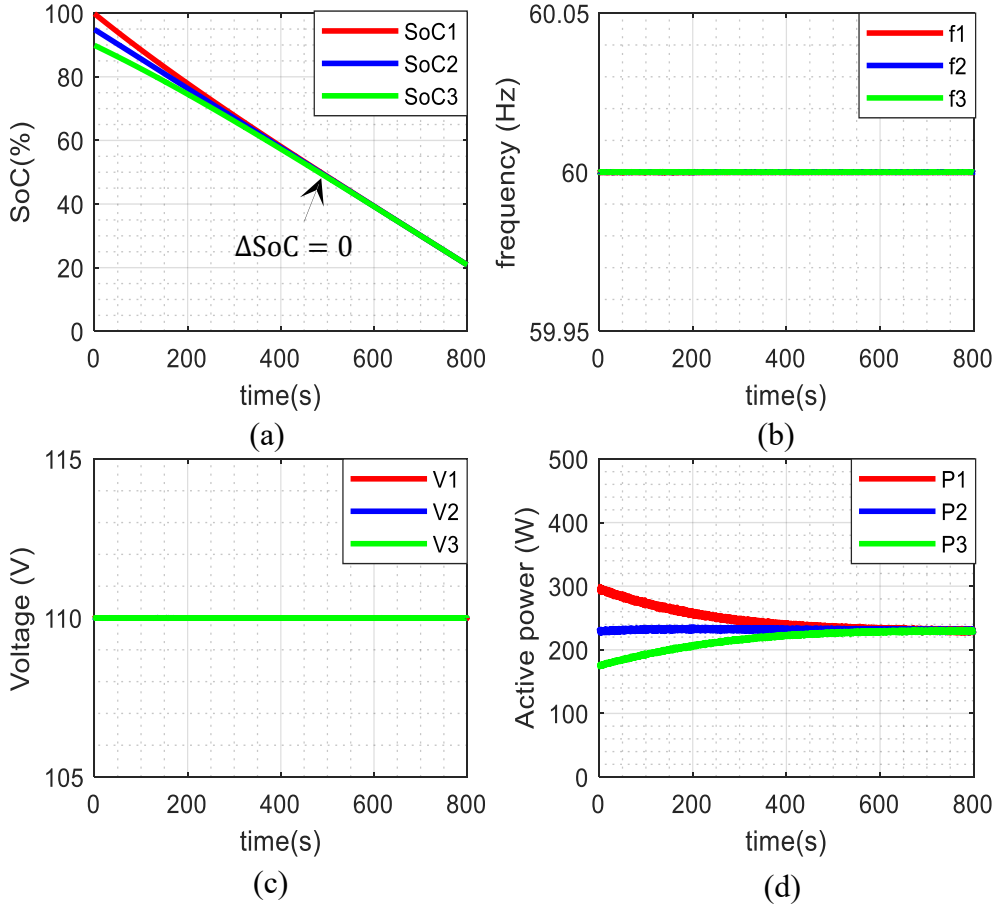

Fig. 15. SoC balancing verification: (a) SoC behavior of the 03 batteries; (b), (c) and (d) measured frequency, RMS voltage and active power at the output of the 03 DGs units.

5. 2. Test 2: Load variation

Second test is realized to verify the effectiveness of the SoC balancing method under load variation. In this test, all resistive loads are reduced from 52Ω to 40 Ω at t=312.4s then are reset to 52Ω at t=510s. Experimental results are reported in Fig. 16. The states of charge of the DESSs are presented in Fig. 16 (a), DESSs frequency and voltage variations are represented in Fig. 16 (b) and Fig. 16 (c) respectively. Active powers of the DESSs are reported in Fig. 16 (d).

Initially all three loads are set at R_{ch}=52Ω. All DESSs supply active power according to their SoCs (Fig 16 (d)) in order to achieve SoC balancing. At t=312.4s, all three loads are reduced to R_{ch}=40Ω which increased the loads demand power. Each DESS supplies more power (Fig. 16 (d)) while ensuring the SoC balancing. The SoCs of the DESSs decreased rapidly (Fig. 16 (a))

due to the increase of the active power of the BESSs. The SoC are synchronized to the same value at 458s (Fig. 16 (a)). Then at 510s, the three loads are reset to R_{ch}=52Ω. The loads demand power drops so the powers of the DESSs. Slight spikes in the voltage and frequency of the DESSs appear during load variation. These peaks are negligible (0.02 V and 0.0003 Hz) compare to the limited variations range (5 V and 0.5 Hz). Frequency and voltage of the DGs (Fig. 16 (b) and Fig. 16 (c) respectively) remain to their nominal values after a load change.

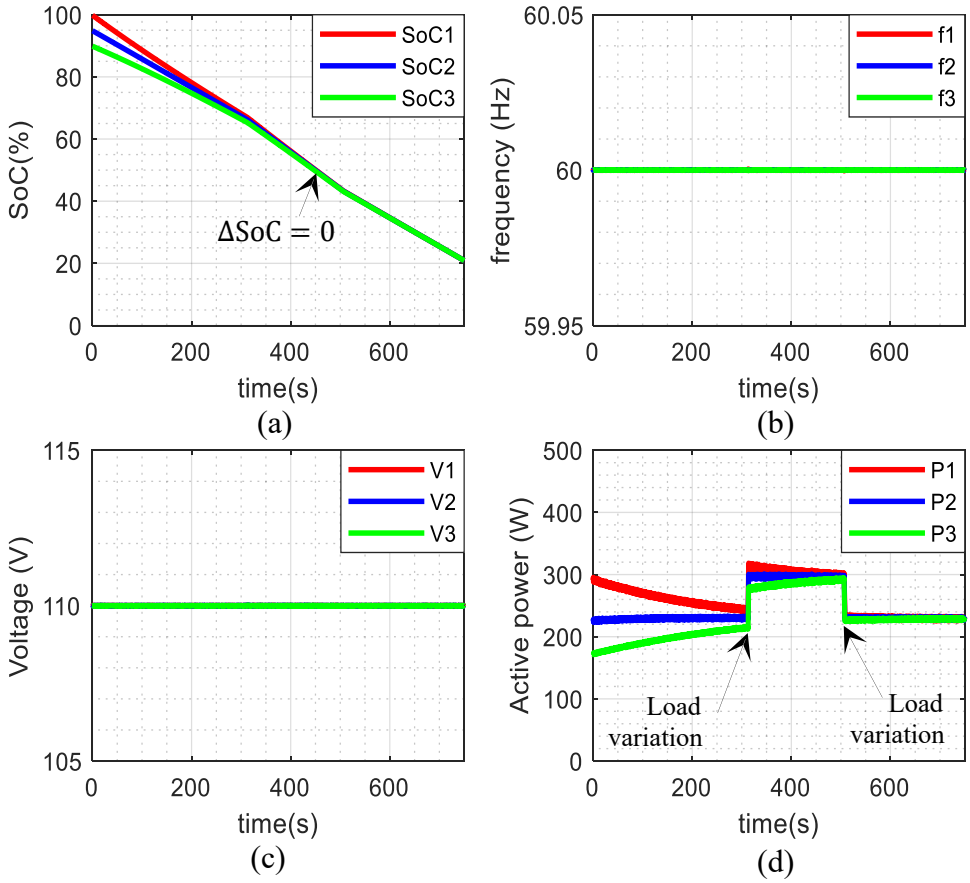

Fig. 16. SoC balancing verification under load variation: (a) SoC behavior of the 03 batteries; (b), (c) and (d) measured frequency, RMS voltage and active power at the output of the 03 DGs units.

5. 3. Test 3: Communication Failure

The third experimental test is devoted to the robustness of the proposed method against communication failures. In order to see the impact of communication failure on the proposed method, a communication link failure between the agent 1 and 2 is simulated as shown in Fig. 8, in the dSPACE at t=200 s. Information exchange between the DESS 1 and the DESS 2 is no

longer possible. Results are reported in Fig. 17. The states of charge of the DESSs are presented in Fig. 17 (a), frequency and voltage of the DESSs are represented in Fig. 17 (b) and Fig. 17 (c) respectively. Active powers of the DESSs are reported in Fig. 17 (d).

Results in Fig. 17 (a) show that despite the loss of communication between the two agents (1 and 2), the SoCs of all DESSs are well synchronized to the same value at 494 s. Communication failure has so no impact on the proposed SoC balancing method. Notice also that the frequency and voltage of the DESSs remained to their nominal (Fig. 17 (b) and (c)) values during the MG operation. Voltage regulation control is also not affected by the loss of the communication link.

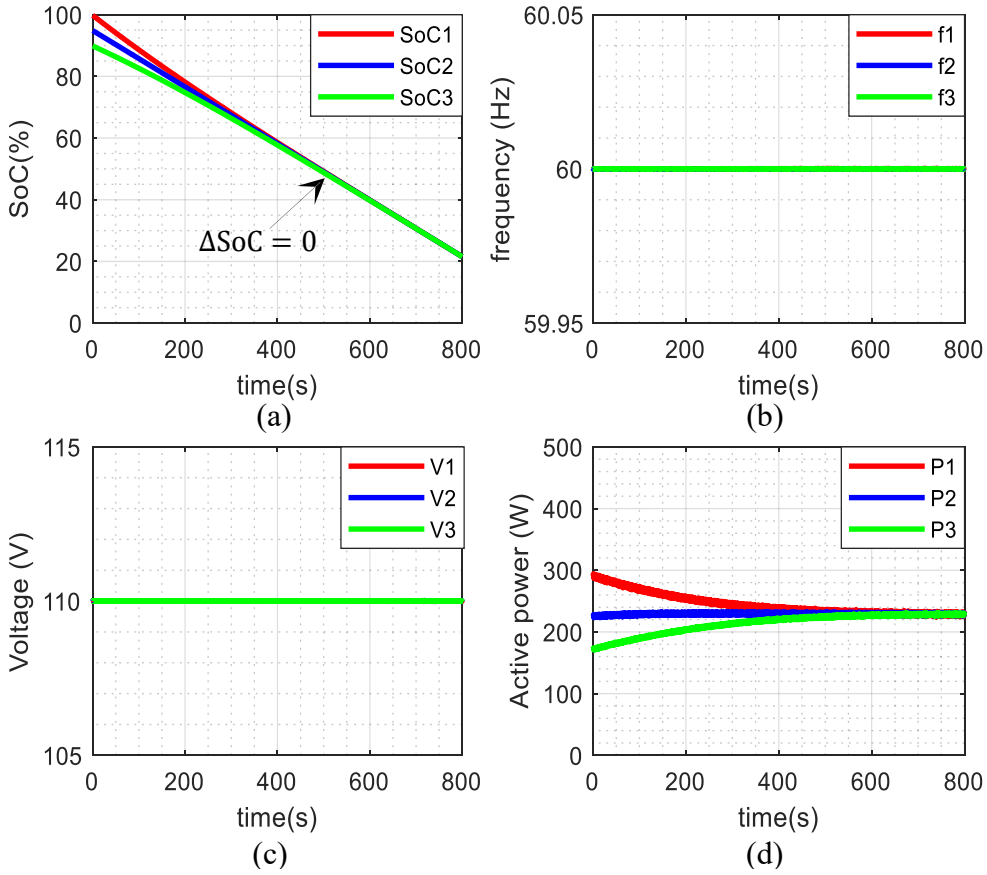

Fig. 17. Impact of communication failure: (a) SoC behavior of the 03 batteries; (b), (c) and (d) measured frequency, RMS voltage and active power at the output of the 03 DGs units.

5. 4. Test 4: Plug and play

In order to investigate the Plug and Play capability, the DESS 3 is disconnected at t=394.6s and reconnected at t=435.9s thanks to a switch. Experimental results are represented in Fig. 18. The states of charge of the DESSs are presented in Fig. 18 (a), frequency and voltage of the DGs are represented in Fig. 18 (b) and Fig. 18 (c) respectively. Active and powers of the DESSs are reported in Fig. 18 (d).

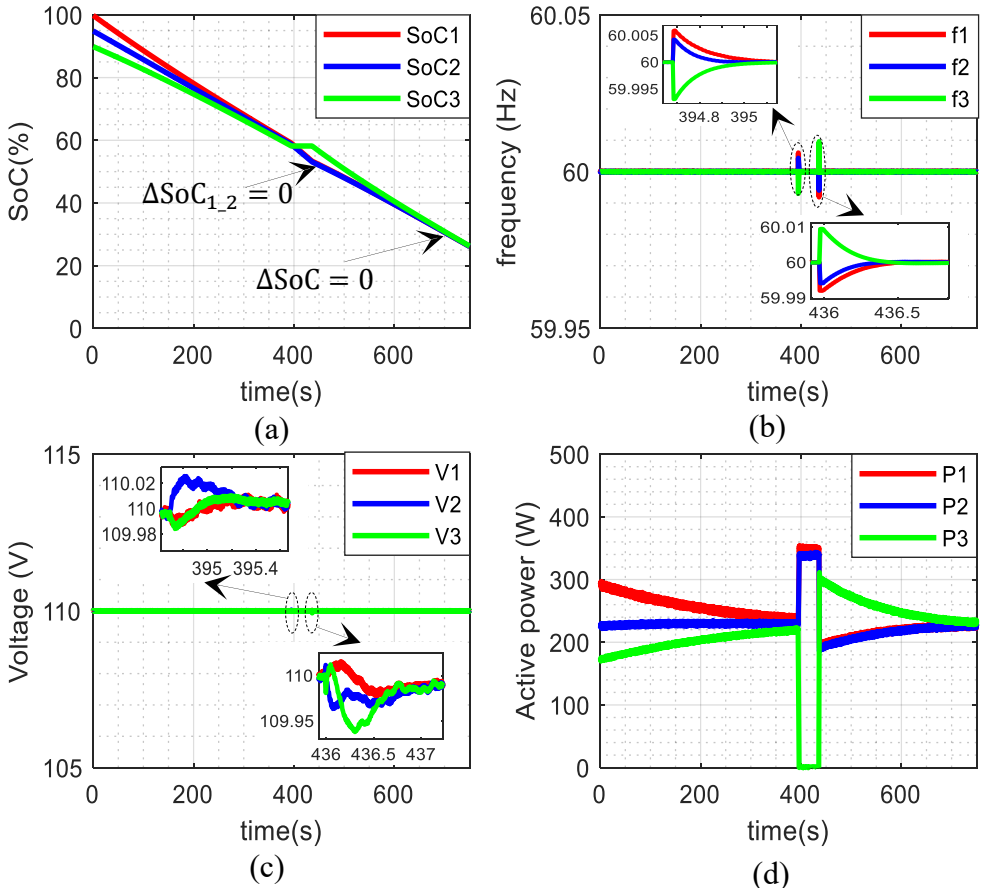

Fig. 18. "Plug and play": (a) SoC behavior of the 03 batteries; (b), (c) and (d) measured frequency, RMS voltage and active power at the output of the 03 DGs units.

Between 0 and 394.6s all DGs are connected to the grid and the DESSs supply powers according to their SoCs. However, at 394.6 s the DESS 3 is disconnected from the MG. Therefore, the DESS 3 shares no power $P_3 = 0$ (Fig. 18 (d)) and the DESS 3 SoC remains to 58%. SoC balancing is ensured only between the DESS 1 and 2 until the DESS 3 is reconnected

at 435.9s. Then, the DESS 3 begins to provide power to the grid. The SoC of the DESS 3 converges to the same value as DESS 1 and 2, resulting in their SoCs being synchronized at 700s (Fig. 18 (a)). It is also worth mentioning that DESSs frequency and voltage (Fig. 18 (b) and Fig. 18 (c) respectively) remain to their nominal values after a disconnection or connection of a DESS even small disturbances are observed but they remain negligible.

5. 5. Test 5: Communication delay

Fourth test is devoted to the impact of time delay in the sparse communication network on the proposed method. By considering the worst-case scenario as in section 4. 5, the impact of a 2 s time delay on the proposed strategy (SoC balancing and voltage regulation) is analyzed in this test using a first-order rational polynomial approximation. In order to study the impact of communication delay on the control in presence of load variations, all three resistive loads are reduced from 52Ω to 40 Ω at t=328s then are reset to 52Ω at t=531s. Experimental results are illustrated in Fig. 19. The SoCs of the DESSs are presented in Fig. 19 (a), frequency and voltage of the DGs are reported in Fig. 19 (b) and Fig. 19 (c) respectively. Active and powers of the DESSs are reported in Fig. 19 (d).

As shown in Fig. 19 (b) and Fig. 19 (c), at startup, the restoration of the voltage and frequency of the DGs to their nominal values takes longer (78s for the voltage and 14s for the frequency) because of the 2s delay time introduced in the control but remained in the permissible ranges of the European norm EN 50160 ($\pm 2\%$ of the nominal value for the frequency and $\pm 10\%$ of the nominal value for the voltage amplitude). However, after the startup, the DGs frequency and voltage are remained to their nominal values and the MG remains stable despite the load variations. SoC balancing is achieved at 459s as illustrated in Fig. 19 (a). The SoC balancing and the voltage regulation convergence speeds after the startup are almost unaffected by the time delay. The proposed method achieves SoC balancing despite the communication network having

a time delay and a 2 s time delay has almost no effect on the dynamic convergence characteristics of the SoC.

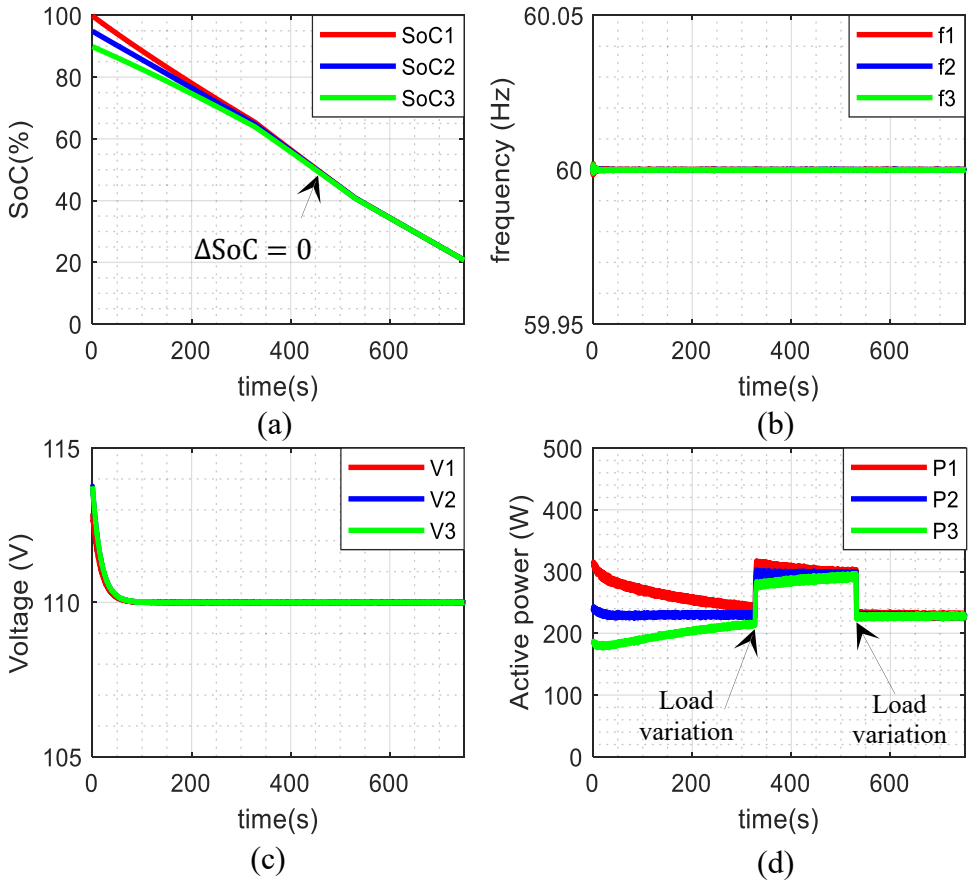

Fig. 19. SoC balancing with 2s time delay: (a) SoC behavior of the 03 batteries; (b), (c) and (d) measured frequency, RMS voltage and active power at the output of the 03 DGs units.

5. 6. Test 6: Comparison with other method

A comparison with the SoC balancing technique used in [5] where an integral control is not also introduced, is realized to evaluate the performance of the proposed scheme. All resistive loads are reduced from 52Ω to 40 Ω at t=314s then are reset to 52Ω at t=508s in both controls. The obtained experimental results are shown in Fig. 20. Results of the proposal are represented to the left and obtained results with the method used in [5] are represented to the right. It can be seen in Fig. 20 (a) and Fig. 20 (b) that SoC balancing is achieved in both controls. However, a static error in the SoCs synchronization control is observed in the results of the method [5],

which remains and increases with load impacts. (ΔSoC=1.53 at 300s and ΔSoC=1.56 at 600s) while for the proposed method this error is eliminated even with load impacts (ΔSoC=1.8 at 300s and ΔSoC=0 at 600s). This static error is usually eliminated by adding an integral control like in [15] or [18], while the proposed method cancels this error without using this integrator.

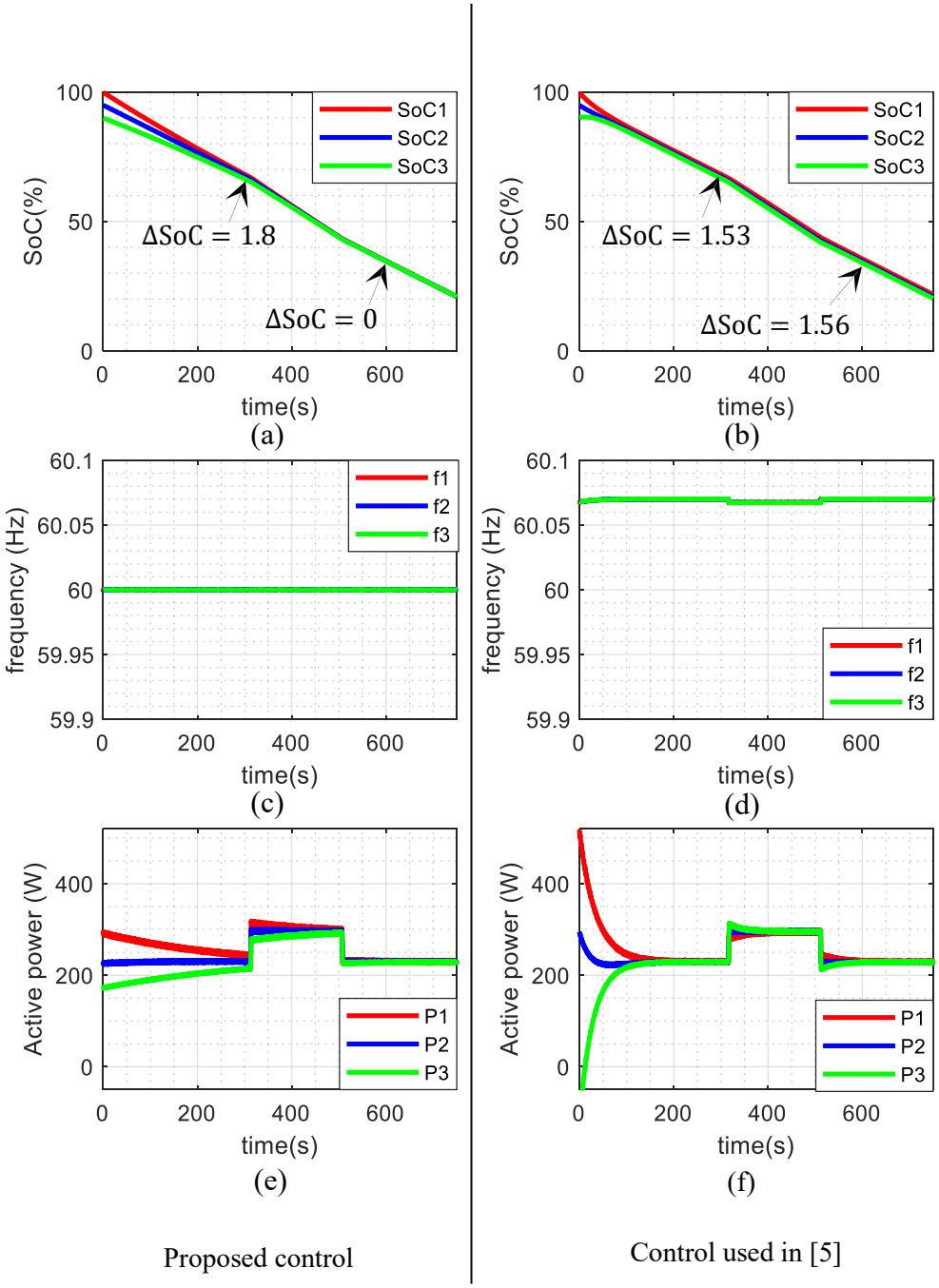

Fig. 20. Comparison between the proposed control and the control used in [5]: (a) and (b) SoC behavior of the 03 batteries, (c) and (d) measured frequency of the DGs, (e) and (f) active power at the output of the 03 DGs units for both controls.

As shown in Fig. 20 (d), the DGs frequencies are not restored to their nominal values and change with load variations. In [5], the frequency of the DGs at steady state depends on the active power of the DG, the error between the SoCs of the DESSs and the maximum allowed deviation value on the frequency. Frequency restoration can be achieved by adding an additional control as consensus control as was done in [15], [18], or [19]. Whereas with the proposed strategy the DGs always operate at nominal frequency (60 Hz) even under load impacts as shown in Fig. 20 (c) without using additional control for frequency regulation.

6. Conclusion

In order to reduce the number of charge/discharge cycles of DESSs to extend their lifetime and maintain the MG stability, this paper focused on a novel distributed control to ensure an effective SoC balancing of the DESSs and frequency restoration with high performance without introducing an integral control which may bring stability issues. The proposed design balances the DESS SoC with accurate output power sharing while providing frequency and voltage regulation with high robustness under communication failure and significant communication delay conditions. The proposed distributed control is validated through MATLAB/Simulink simulation and on an experimental setup. The simulation and experimental results show the effectiveness of the proposed power management control in charging mode, discharging mode, large load change scenario, communication failure, communication delay, presence of variable renewable energy and “plug and play” working conditions.

References

[1] N. Khefifi, A. Houari, M. Machmoum, A. Saim, et M. Ghanes, « Generalized IDA-PBC Control using Enhanced Decoupled Power Sharing for Parallel Distributed Generators in Standalone Microgrids », *IEEE Journal of Emerging and Selected Topics in Power Electronics*, p. 1-1, 2020, doi: 10.1109/JESTPE.2020.3034464.

[2] G. Shi, H. Han, Y. Sun, Z. Liu, M. Zheng, et X. Hou, « A Decentralized SOC Balancing Method for Cascaded-Type Energy Storage Systems », *IEEE Transactions on Industrial Electronics*, vol. 68, nº 3, p. 2321-2333, mars 2021, doi: 10.1109/TIE.2020.2973889.

[3] L. Chang, W. Zhang, S. Xu, et K. Spence, « Review on distributed energy storage systems for utility applications », *CPSS Transactions on Power Electronics and Applications*, vol. 2, nº 4, p. 267-276, déc. 2017, doi: 10.24295/CPSSTPEA.2017.00025.

[4] D. Wu, F. Tang, T. Dragicevic, J. C. Vasquez, et J. M. Guerrero, « A Control Architecture to Coordinate Renewable Energy Sources and Energy Storage Systems in Islanded Microgrids », *IEEE Transactions on Smart Grid*, vol. 6, nº 3, Art. nº 3, mai 2015, doi: 10.1109/TSG.2014.2377018.

[5] C. Li, E. A. A. Coelho, T. Dragicevic, J. M. Guerrero, et J. C. Vasquez, « Multiagent-Based Distributed State of Charge Balancing Control for Distributed Energy Storage Units in AC Microgrids », *IEEE Transactions on Industry Applications*, vol. 53, nº 3, Art. nº 3, mai 2017, doi: 10.1109/TIA.2016.2645888.

[6] C. Huang, S. Weng, D. Yue, S. Deng, J. Xie, et H. Ge, « Distributed cooperative control of energy storage units in microgrid based on multi-agent consensus method », *Electric Power Systems Research*, vol. 147, p. 213-223, juin 2017, doi: 10.1016/j.epsr.2017.02.029.

[7] M.-A. Hamidan et F. Borousan, « Optimal planning of distributed generation and battery energy storage systems simultaneously in distribution networks for loss reduction and reliability improvement », *Journal of Energy Storage*, vol. 46, p. 103844, févr. 2022, doi: 10.1016/j.est.2021.103844.

[8] D. Li, Z. Wu, B. Zhao, et L. Zhang, « An Improved Droop Control for Balancing State of Charge of Battery Energy Storage Systems in AC Microgrid », *IEEE Access*, vol. 8, p. 71917-71929, 2020, doi: 10.1109/ACCESS.2020.2987098.

[9] N. L. Díaz, A. C. Luna, J. C. Vasquez, et J. M. Guerrero, « Centralized Control Architecture for Coordination of Distributed Renewable Generation and Energy Storage in Islanded AC Microgrids », *IEEE Transactions on Power Electronics*, vol. 32, nº 7, Art. nº 7, juill. 2017, doi: 10.1109/TPEL.2016.2606653.

[10] R. Zhang, A. V. Savkin, et B. Hredzak, « Centralized nonlinear switching control strategy for distributed energy storage systems communicating via a network with large time delays », *Journal of Energy Storage*, vol. 41, p. 102834, sept. 2021, doi: 10.1016/j.est.2021.102834.

[11] J. Hu et P. Bhowmick, « A consensus-based robust secondary voltage and frequency control scheme for islanded microgrids », *International Journal of Electrical Power & Energy Systems*, vol. 116, p. 105575, mars 2020, doi: 10.1016/j.ijepes.2019.105575.

[12] H. Ali, A. Hussain, V.-H. Bui, et H.-M. Kim, « Consensus Algorithm-Based Distributed Operation of Microgrids During Grid-Connected and Islanded Modes », *IEEE Access*, vol. 8, p. 78151-78165, 2020, doi: 10.1109/ACCESS.2020.2989457.

[13] M. A. Shahab, B. Mozafari, S. Soleymani, N. M. Dehkordi, H. M. Shourkaei, et J. M. Guerrero, « Distributed Consensus-Based Fault Tolerant Control of Islanded Microgrids », *IEEE Transactions on Smart Grid*, vol. 11, nº 1, Art. nº 1, janv. 2020, doi: 10.1109/TSG.2019.2916727.

[14] J. Khazaei et Z. Miao, « Consensus Control for Energy Storage Systems », *IEEE Transactions on Smart Grid*, vol. 9, nº 4, Art. nº 4, juill. 2018, doi: 10.1109/TSG.2016.2624144.
[15] A. M. Shotorbani, B. Mohammadi-Ivatloo, L. Wang, S. Ghassem-Zadeh, et S. H. Hosseini, « Distributed secondary control of battery energy storage systems in a stand-alone microgrid », *IET Generation, Transmission & Distribution*, vol. 12, nº 17, p. 3944-3953, 2018, doi: 10.1049/iet-gtd.2018.0105.
[16] O. Palizban et K. Kauhaniemi, « Distributed cooperative control of battery energy storage system in AC microgrid applications », *Journal of Energy Storage*, vol. 3, p. 43-51, oct. 2015, doi: 10.1016/j.est.2015.08.005.
[17] Y. Guan, J. C. Vasquez, et J. M. Guerrero, « Coordinated Secondary Control for Balanced Discharge Rate of Energy Storage System in Islanded AC Microgrids », *IEEE Transactions on Industry Applications*, vol. 52, nº 6, Art. nº 6, nov. 2016, doi: 10.1109/TIA.2016.2598724.
[18] S. Ouoba, A. Houari, et M. Machmoum, « Robust SoC Balancing Method for Distributed Storage based Islanded Microgrids », in *IECON 2021 – 47th Annual Conference of the IEEE Industrial Electronics Society*, oct. 2021, p. 1-6. doi: 10.1109/IECON48115.2021.9589165.
[19] A. M. Shotorbani, S. Ghassem-Zadeh, B. Mohammadi-Ivatloo, et S. H. Hosseini, « A distributed secondary scheme with terminal sliding mode controller for energy storages in an islanded microgrid », *International Journal of Electrical Power & Energy Systems*, vol. 93, p. 352-364, déc. 2017, doi: 10.1016/j.ijepes.2017.06.013.
[20] M. Dahmardeh et Z. Xi, « Probabilistic state-of-charge estimation of lithium-ion batteries considering cell-to-cell variability due to manufacturing tolerance », *Journal of Energy Storage*, vol. 43, p. 103204, nov. 2021, doi: 10.1016/j.est.2021.103204.
[21] J. Snoussi, S. Ben Elghali, M. Zerrougui, M. Bensoam, M. Benbouzid, et M. F. Mimouni, « Unknown input observer design for lithium-ion batteries SOC estimation based on a differential-algebraic model », *Journal of Energy Storage*, vol. 32, p. 101973, déc. 2020, doi: 10.1016/j.est.2020.101973.
[22] Y.-J. Ee, K.-S. Tey, K.-S. Lim, P. Shrivastava, S. B. R. S. Adnan, et H. Ahmad, « Lithium-Ion Battery State of Charge (SoC) Estimation with Non-Electrical parameter using Uniform Fiber Bragg Grating (FBG) », *Journal of Energy Storage*, vol. 40, p. 102704, août 2021, doi: 10.1016/j.est.2021.102704.
[23] Y. Khayat *et al.*, « On the Secondary Control Architectures of AC Microgrids: An Overview », *IEEE Transactions on Power Electronics*, vol. 35, nº 6, p. 6482-6500, juin 2020, doi: 10.1109/TPEL.2019.2951694.
[24] U. B. Tayab, M. A. B. Roslan, L. J. Hwai, et M. Kashif, « A review of droop control techniques for microgrid », *Renewable and Sustainable Energy Reviews*, vol. 76, p. 717-727, sept. 2017, doi: 10.1016/j.rser.2017.03.028.
[25] A. B. Shyam, S. Anand, et S. R. Sahoo, « Effect of Communication Delay on Consensus-Based Secondary Controllers in DC Microgrid », *IEEE Transactions on Industrial Electronics*, vol. 68, nº 4, p. 3202-3212, avr. 2021, doi: 10.1109/TIE.2020.2978719.